Journal of ASTM International, June 2005, Vol. 2, No. 6
Paper ID JAI12390
Available online at www.astm.org

S. Abolhassani,[1] *R. Restani,*[1] *T. Rebac,*[1] *F. Groeschel,*[1] *W. Hoffelner,*[1] *G. Bart,*[1] *W. Goll,*[2] *and F. Aeschbach*[3]

TEM Examinations of the Metal-Oxide Interface of Zirconium Based Alloys Irradiated in a Pressurized Water Reactor

ABSTRACT: Metal-oxide interfaces of three different materials irradiated in a pressurized water reactor have been analyzed by TEM and AEM. Standard Zircaloy-4, low-tin Zircaloy-4, and Zr-2.5%Nb were used for this study. The microstructure of the material on the two sides of the metal-oxide interface, the geometry of the interface, the distribution of different alloying elements, and the oxygen profile have been examined in each material. Results of the examinations showed that the three materials had different microstructure and oxygen distribution on the two sides of the metal-oxide interface. In particular, the following parameters were noticed: a) the geometry of the interface seems to be of a different nature in the case of Zr-2.5%Nb alloy. Unlike the Zircaloy-4 alloys, which show an undulated interface, this material has a "jigsaw" type interface. This point is discussed, and its role on the oxidation is considered. b) Hydrides are observed and analyzed in the vicinity of the interface in the case of low-tin Zircaloy-4, and it is shown that they can have an influence on the occurrence of cracks in this material. c) The origins of stress are discussed, and it is shown that it can have different sources. The crystal structure of the oxides is mainly monoclinic. A tetragonal oxide is observed at some regions, in particular in the standard Zircaloy-4.

KEYWORDS: zirconium alloys, oxidation, metal-oxide interface, TEM observations, EDS mapping

Introduction

Irradiation effects on the oxidation rate of zirconium alloys have been examined by several studies, and the common agreement is that the material can have a different behavior after a long-term stay in the reactor [1–3]. These studies have shown that the difference in behavior can have several reasons. Observations on one material under specific reactor conditions do not always extrapolate or generalize to other conditions. This conclusion would imply that the mechanism of oxidation in the reactor deviates at a certain stage from that of the oxidation in the autoclave. Additionally, it implies more than one mechanism is involved in the oxidation of the material in the reactor, especially at different stages of oxidation.

The oxidation of zirconium alloys at high temperatures is governed by the diffusion of the oxidizing species to the metal-oxide interface [4,5]. Stresses in the oxide due to the Pilling-Bedworth parameter (for this material, approx. 1.56) are compressive, and as an example Zircaloy-4 (metallic phase) at the interface is reported to be under a tensile stress [6] and the oxide under a compressive stress in the range of 200–500 MPa [7]. In the case of precipitate containing alloys, metallic precipitates do not oxidize before they are totally surrounded by the oxide [8]. The monoclinic zirconia phase is the predominant phase in the oxide. However,

Manuscript received 3 May 2004; accepted for publication 6 December 2004; published June 2005. Presented at ASTM Symposium on Zirconium in the Nuclear Industry: Fourteenth International Symposium on 13–17 June 2004 in Stockholm, Sweden; B. Kammenzind and P. Rudling, Guest Editors.
[1] Paul Scherrer Institut, Laboratory for Materials Behaviour, 5232 Villigen-PSI, Switzerland.
[2] Framatome ANP GmbH, Postfach 3220, 91050 Erlangen, Germany.
[3] Kernkraftwerk Gösgen-Däniken, Däniken 4658, Switzerland.

different researchers have found different concentrations of tetragonal and cubic zirconia in the vicinity of the interface [9–11]. The observations by different authors describe these phases to be present in the vicinity of the interface. As the oxidation rate is governed by the diffusion of oxidizing species to the metal-oxide interface, the oxidation rate is expected to slow down with the increasing oxide thickness. This is the case for the early stages of oxidation, which have parabolic or cubic kinetics. After a given period of time however, the oxidation rate becomes linear and independent from the total thickness of the oxide layer. This phenomenon is explained by the appearance of different rapid roots created in the course of oxidation, due to the cracking of the oxide layer, the dissolution of the oxide, etc. for the oxidizing species to reach the metal-oxide interface [12–14]. The above observations have been performed on both autoclaved and irradiated materials. After an initial period of exposure, the oxide growth in the reactor is faster than that in the autoclave.

The dissolution of precipitates under irradiation is considered one of the causes of faster oxidation. Other causes are expected to be responsible for this discrepancy, such as hydride rims and heat flux. As the last oxide formed is always at the metal-oxide interface, examining the interface might indicate the causes for this change of behavior.

The resolution limit of different structural analysis methods used for the examination of the metal-oxide interface varies from the micrometer levels (e.g., for synchrotron radiation) to nanometer level for transmission electron microscope (TEM). The results of the different techniques should provide complementary information for a better understanding of the phenomena.

TEM observations of the interface are useful in this respect, as they bring structural information with a high spatial resolution. In a previous study the metal-oxide interface of autoclaved material was analyzed [15], while in the present study, an attempt is made to analyze the metal-oxide interface of irradiated alloys.

Materials and Methods

Three different alloys irradiated in a pressurized water reactor (PWR), listed in Table 1, are used for this study. The irradiation data, number of cycles in the reactor, as well as the oxide thickness of the TEM sample and its axial position on the rod are indicated. The maximum oxide thickness of the rod and the mean secondary phase particle (SPP) size of each material are also provided. These materials have been characterized in the framework of other projects in the laboratory. The objective of the present study is to focus on the microstructural analysis of the metal-oxide interface by TEM and by analytical electron microscopy (AEM). The chemical composition and heat treatment of the alloys are provided in Table 2.

Two methods are used for the sample preparation: conventional ion beam milling and focused ion beam milling (FIB). Details of sample cutting and cleaning as well as the orientation of the samples are given in Appendix I. For conventional ion beam milling, a Baltec RES010 instrument was used. The samples were prepared using a procedure developed by the company for metal-oxide interface preparation. The technique is based on very accurate thinning and surface polishing of the sample prior to ion milling. The milling procedure (sample rotation, gun incidence angle, and milling times) is very accurately programmed to obtain an optimum result. Samples prepared by this conventional ion beam milling showed thickness variations and were not convenient for chemical analysis and comparison of the two sides of the interface. When possible, FIB was used to prepare the samples. In this method, a very thin segment is prepared from the specimen by focusing an ion beam and literally cutting the segment out of the sample.

This method provides samples with a homogeneous thickness appropriate for X-ray microanalysis; two of the materials were prepared with this method. An FEI Strata DB 235 dual beam™ (DB) focused ion beam (FIB) workstation has been used for these experiments. The TEM specimens were prepared by milling an electron-transparent sample (about 20 μm long, 5 μm wide, and 100 nm thick) from a bulk sample (lift-off method). For this purpose, the materials were sent outside the hot-laboratory. Only two samples were below the exemption level of activity and could be prepared outside the hot laboratory using the FIB technique. These samples were low-tin Zircaloy-4 and Zr-2.5%Nb. It is worth mentioning that the contamination from milling the sample in a FIB was negligible.

TABLE 1—*Materials used for the examination of the metal-oxide interface. The rod maximum oxide thickness was obtained from non-destructive tests by Eddy Current method. The thickness of the segment used for TEM analysis was measured by scanning electron microscopy.*

Material	No. of Cycles (rod no.)	Burn up MWd/Kg U	Fluence Estimated n/cm^2 $E > 0.821MeV$	Sample Elevation from the Bottom (mm)	Rod Max. Oxide Thickness μm	TEM Sample Oxide Thickness μm	Hydrogen Pick-up (ppm)	SPP Mean size (nm)
Zircaloy-4 standard	4	51.4	3×10^{21}	260	97	10	260–500	180
Low-tin Zircaloy-4	4	51.1	10.3×10^{21}	1468	59	25	367–460	190
Zr-2.5%Nb	3	41.4	8.3×10^{21}	869	16	6.9	70	n.a.

n.a.: not available.

TABLE 2—*Chemical composition of the alloys used and the final heat treatment of the cladding material.*

Material	Sn (wt%)	Fe (wt%)	Cr (wt%)	Nb (wt%)	Si (ppm)	C (ppm)	O (ppm)	H (ppm)	H.T.
Zircaloy-4 standard	1.52	0.21	0.106			140	1260	7	507°C SRA
Low-tin Zircaloy-4	1.20	0.22	0.107			140	1730	8	504°C SRA
Zr-2.5%Nb		0.07		2.5	60	180	1170	10	500°C PRX

H.T.: heat treatment, SRA: stress relieve annealed, and PRX: partially recrystallized condition.

A JEOL2010 transmission electron microscope operating at 200 keV (LaB_6 filament) was used. The microscope was equipped with an Oxford Instrument's Energy Dispersive X-ray Spectrometer (EDS) with minimum resolution of 132 eV. A "Link-ISIS" software was used for this detector. For quantitative analysis purposes, a calibration was performed using a pure zirconium oxide powder and a film as standards. The details of this point are presented in the discussion. For some observations, a Philips CM200 operating at 200 keV (LaB_6 filament) has been used. This microscope has a point resolution of 0.24 nm. The electron diffraction patterns for each structure were calculated using the JEMS software developed by P. Stadelmann (Ecole Poyltechnique Fédérale de Lausanne). Crystallographic data for identifying different phases are provided in Appendix II.

Results of TEM Observations

Standard Zircaloy-4

The metal-oxide interface of the standard Zircaloy-4 is presented in Fig. 1. This material was prepared by ion beam milling. The oxide structure near the interface is columnar, the grains have an average width of 20 nm, and the length of the columns is of the order of 100 nm. The high resolution image of the same region shows the atomic structure of the oxide. The crystal structure of the oxide is mainly monoclinic. However, a detailed examination shows a tetragonal oxide present in small quantity in the grain boundary of the monoclinic structure. Tetragonal oxide usually is present in fine grains, and it is hard to image its single grains; a nanodiffraction of a relatively large single grain can be seen in Fig. 2. The oxide structure shows many defects and a large dislocation density. This high dislocation density could be related to the radiation damage but also to the stress in the oxide, as this latter parameter exists regardless of the level of irradiation.

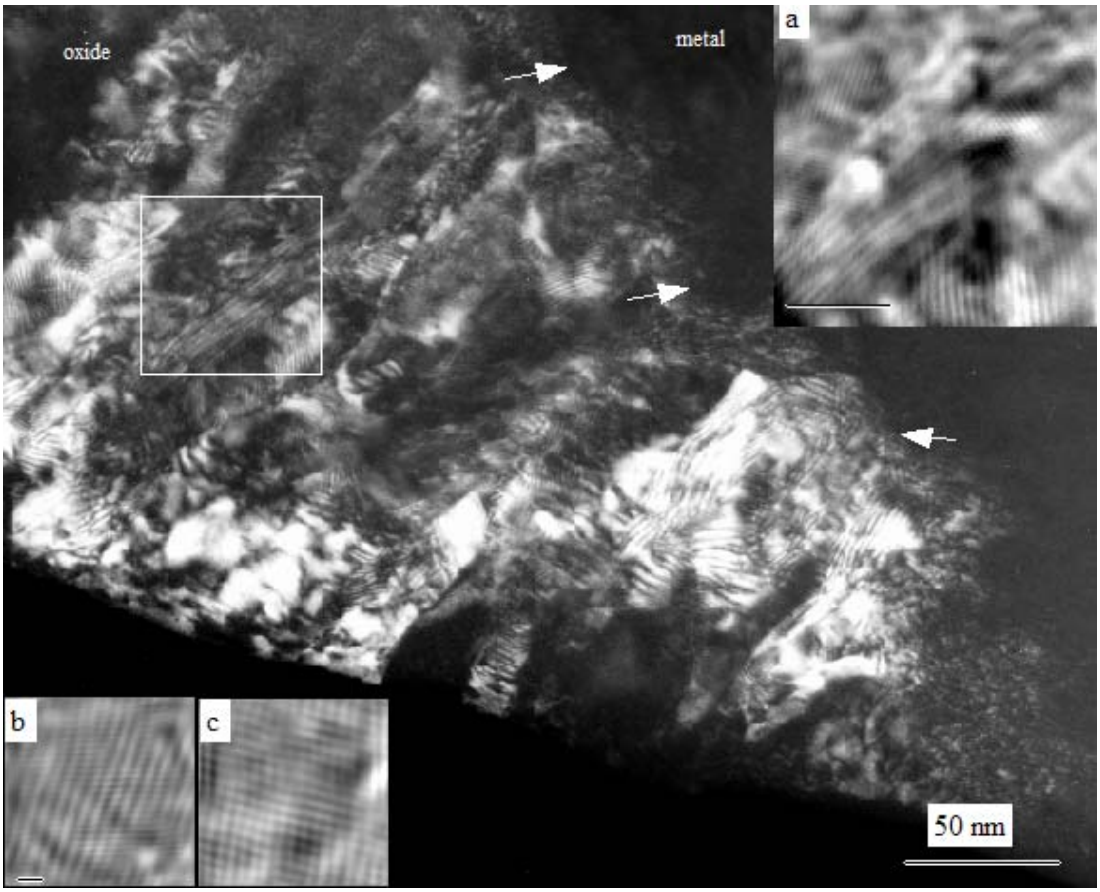

FIG. 1—*TEM dark field image of the metal-oxide interface of the standard Zircaloy-4 irradiated for 4 cycles. The bright field contrast of the selected region is shown in the inset* a*, at higher magnification. The microstructure of the oxide can be observed. The insets* b *and* c *are selected regions of a showing the atomic arrangement of the oxide. Arrows point to the interface. Scale bar in* a *represents 20 nm and in* b *and* c *represents 2 nm.*

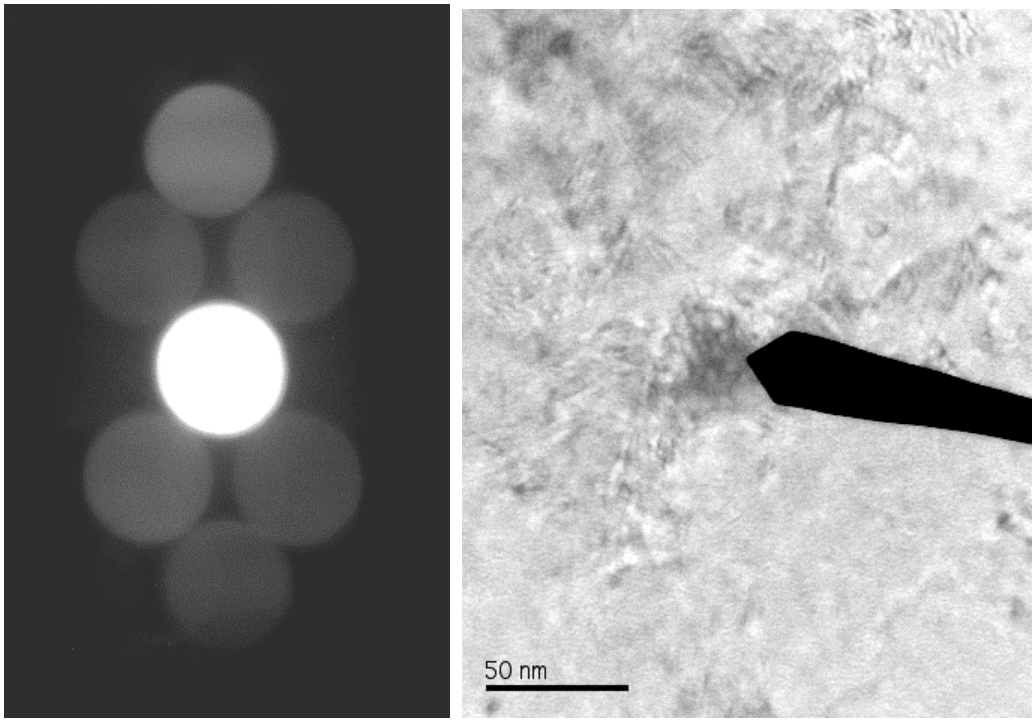

FIG. 2—*Nano-diffraction of a tetragonal zirconia grain, and the corresponding bright field image of the grain, in the same material as in Fig. 1. The diffraction shows a [100] zone axis of tetragonal. The grain size of this oxide is about 30 nm.*

The thickness of the oxide in this irradiated sample was approximately 10 μm. The waterside oxide also showed a columnar structure similar to the interface oxide (Fig. 3). The columnar grains were on the average 25 nm wide and can be as long as 400 nm.

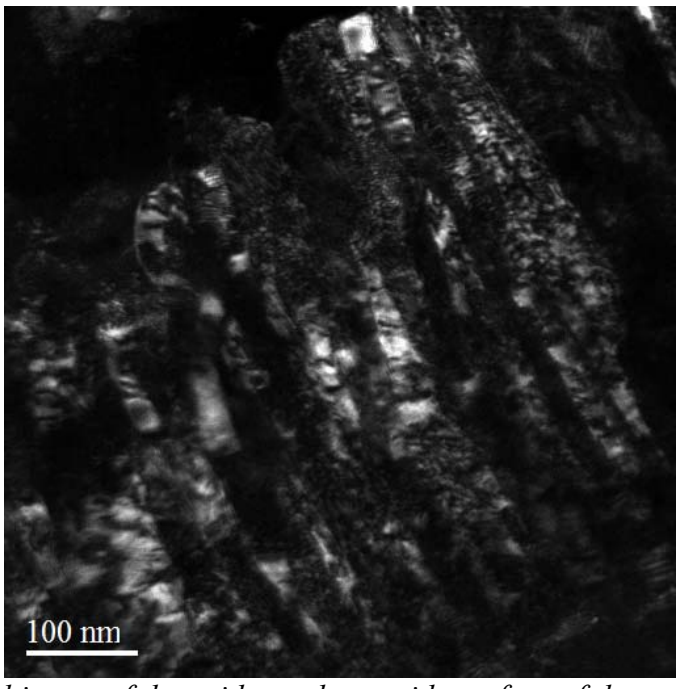

FIG. 3—*Dark field image of the oxide on the outside surface of the standard Zircaloy-4. The columnar grains are also seen in this region.*

The metal-oxide interface of another specimen of this material is shown in Fig. 4*a*. The oxide grains in this region are equi-axed. This observation shows that the oxide morphology of the standard Zircaloy-4 is not always columnar. From the analysis of the oxide in this region it can be observed that the oxidation has proceeded in the metal grain boundary. This grain boundary oxidation is not often reported. The profile of oxygen is not measured for this material since the thickness variation of the thin foil would induce an error in the oxygen quantification. The elemental map of the same region is shown in Fig. 4*c*. In the metal side of the oxide a precipitate can be observed. In addition to the above observations, we found very small hydride needles perpendicular to the interface (not shown here). The metal-oxide interface of this material was evaluated to be undulated. However, in the region shown in Fig. 4 the interface can be characterized as planar.

Low-Tin Zircaloy-4

Thin foils for this material have been prepared by FIB. An overall view of the metal-oxide interface of this material can be observed in Fig. 5*a*. The interface of this material shows large stresses and is undulated, at some places having a sinusoidal form. The analysis of the electron diffraction patterns of the interface has shown the presence of these stresses in the interface (Fig. 5*b*). This has also been verified by high resolution transmission electron microscopy (not shown here). The geometry of the interface is important, as the stress distribution on the two sides of the interface depends on this parameter and will influence the oxidation behavior. This point will be discussed later.

The metal side of the interface in this material shows platelet type precipitates that can be considered as hydrides (Fig. 5*a*). The diffraction pattern of these platelets has been analyzed in order to characterize the platelets (Fig. 5*d*). Usually a δ-hydride ($ZrH_{1.66}$) or a γ-hydride (ZrH) is reported in the α-Zr matrix. The diffraction of the platelet in this region indicates a value of the lattice spacing of 0.29 nm. Though the metal side of the interface could be under a tensile stress, it is surprising to have such a large stress for the hydride. This spacing corresponds to the (111) plane of the cubic zirconia. To clarify this problem, another FIB specimen was analyzed to examine the nature of platelets in the metal side of the interface. A large quantity of such platelets was observed in the material, and the d-spacing was measured to be 0.276 nm. The point analysis of these platelets did not show large oxygen concentration expected to be present in the zirconia. Also, the lattice spacing of 0.276 nm corresponds to the (111) plane of δ-hydride or the (101) plane of ε-hydride. The conclusion was that the platelets were hydrides, and it could be possible that the hydrides in the vicinity of the interface show a preferential oxidation. This point should be further examined in the future on other materials. The bright field image of a grain showing typical c-type dislocations is presented at higher magnification in Fig. 5*c*. In this grain, similar hydride type platelets can be observed that are mostly parallel to the (001) planes of α-Zr. Certain platelets are also observed in the grain boundary of the α-Zr matrix. A higher magnification image of the metal-oxide interface is shown in Fig. 6. Oxide grains are equi-axed in this region.

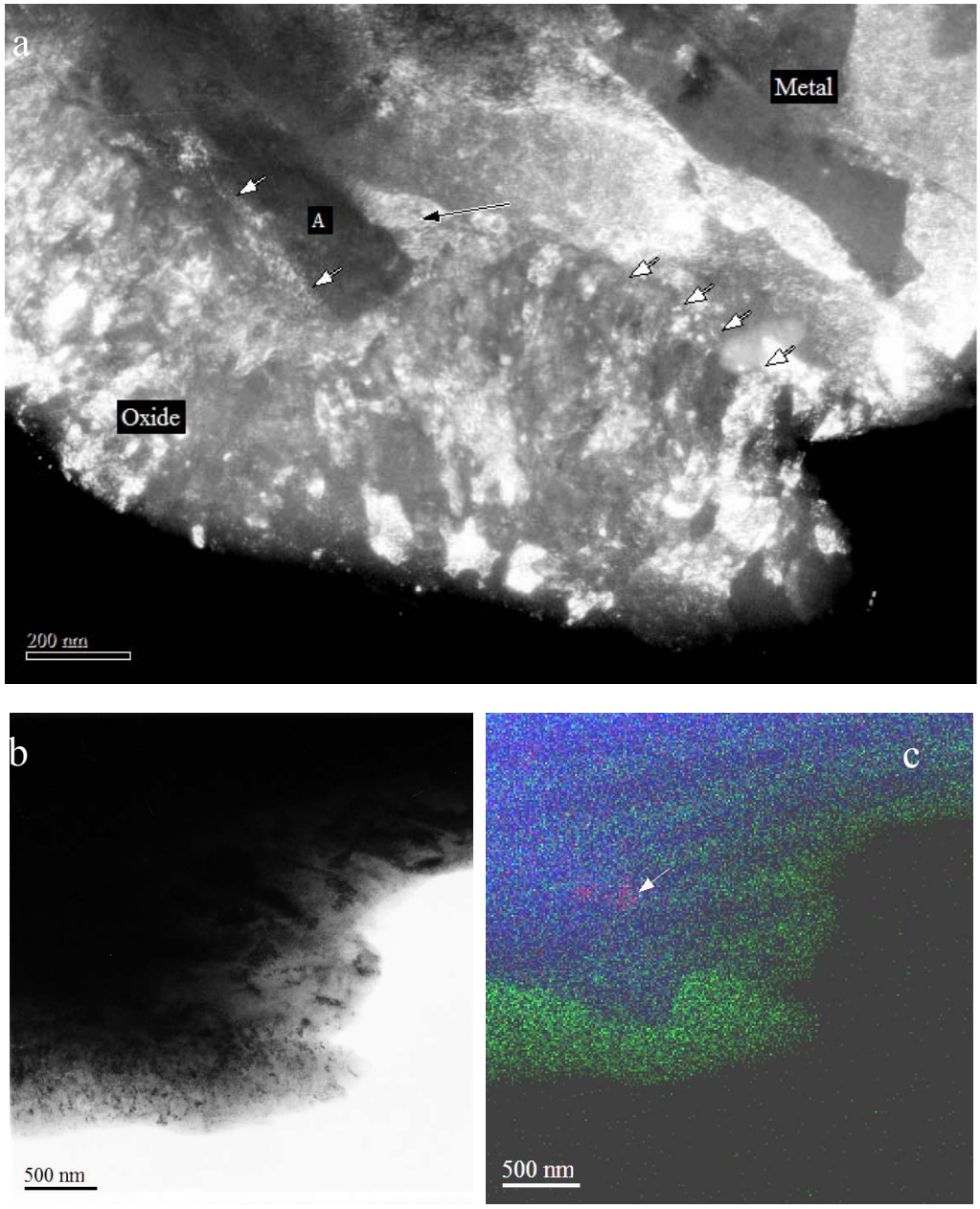

FIG. 4—a*) Dark field image of the metal-oxide interface of the standard Zircaloy-4. White arrows indicate the interface, black arrow indicates intergranular oxide; region A has a metallic diffraction pattern (α-Zr).* b*) Bright field contrast of the same region as* a *and* c. c*) EDS map of Zirconium (Blue), Oxygen (Green), and Cr (red). Arrow indicates the position of the precipitate in the metal side of the interface.*

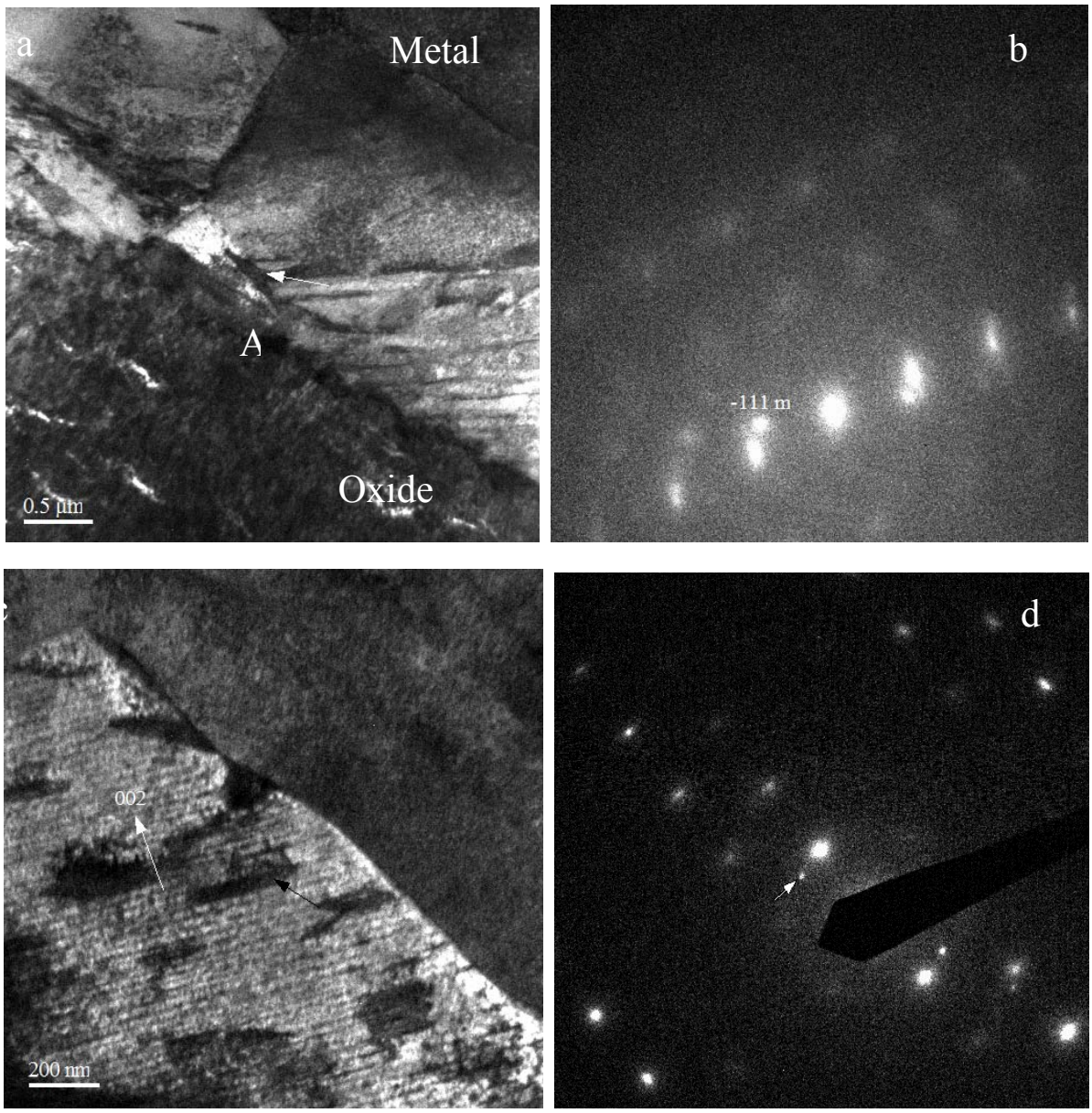

FIG. 5—a*) Bright field image of the metal-oxide interface of the Low-tin Zircaloy-4, irradiated for four cycles. The metal side of the interface shows platelets as indicated by the arrow.* b*) Diffraction pattern of the interface in a region such as that indicated by A in Fig. 5*a*. Two diffractions spots are observed, one corresponding to the metal and the other to the oxide. The diffraction spot of the oxide corresponds to the (-111) of monoclinic oxide as indicated.* c*) The dislocation structure in the metal side of the interface. The hydride platelets in this grain are observed oriented along the (001) planes (black arrow).* d*) Diffraction pattern from the platelet indicated by arrow in Fig. 4*a*. Small arrow in this image indicates the diffraction spot from the platelet. This corresponds to a d-spacing of 0.29 nm.*

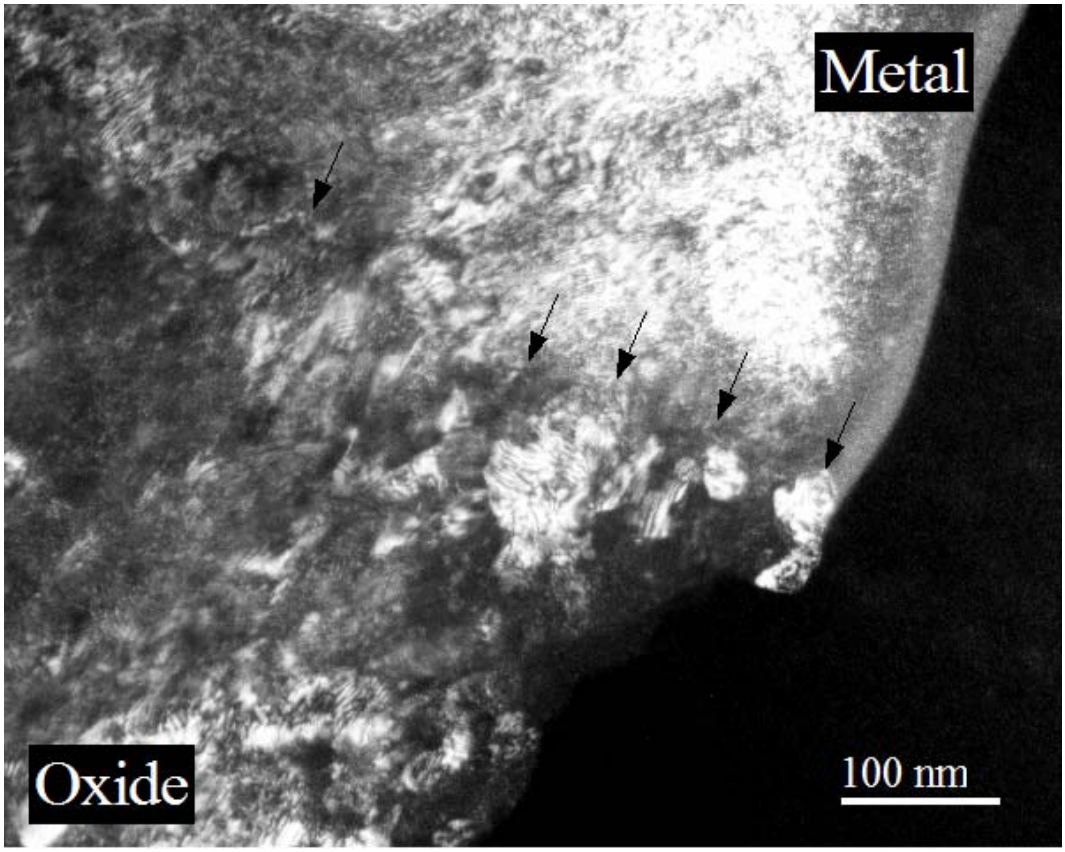

FIG. 6—*Metal-oxide interface of the Low-tin Zircaloy-4, irradiated for four cycles. Dark field contrast showing the interface and the oxide grains. The oxide grains in this region have an average width of 20 nm and an average length of 60 nm.*

As the hydrides are observed close to the interface it is expected that a trace of oxidized hydride would be present in the oxide side of the interface. An attempt has been made to further examine this point by performing a detailed analysis of the two sides of the interface. Figure 7*a* represents a hydride at the metal side of the interface at a distance of 1.6 μm from it. The dark field contrast of this hydride is shown in Fig. 7*b*. Other platelets are also observed in the same region. The diffraction of these platelets corresponds to the (220) reflection of ε-hydride. Figure 7*c* shows the oxide side of the interface. In this oxide, less dense regions can be observed, which are usually characterized as cracks. However, they show a similar size and shape as the platelets, and a higher magnification image of these regions (Fig. 7*d*) shows the small grains as observed in the platelets in the metal side of the interface. The crystal structure of the oxide in these less dense regions corresponds to monoclinic zirconia.

The oxide grains in this material show two types of morphology; columnar and equi-axed grains are seen. The columnar grains can be as long as 500 nm and have an average width of 30 nm (Fig. 8). These columnar oxides are mostly free from cracks and are usually parallel to the direction of the oxide growth. The analysis of their diffraction shows a monoclinic structure. Such grains are also observed at the metal-oxide interface (not shown here). The equi-axed oxide grains are dispersed over the whole oxide, and they show cracks in their grain boundaries.

The EDS map of the interface of this material shows a very distinct boundary between the oxide and the metal (Fig. 9*a*). This material shows a high oxygen concentration in the metal side

of the interface. Figure 9*b* indicates the EDS point analysis for oxygen and zirconium concentration of the material on the two sides of the interface. It must be noted that the oxygen signal can be absorbed by zirconium, and calibrations are necessary in order to obtain reasonable results, details of these calibrations are given in the discussion on the chemical composition.

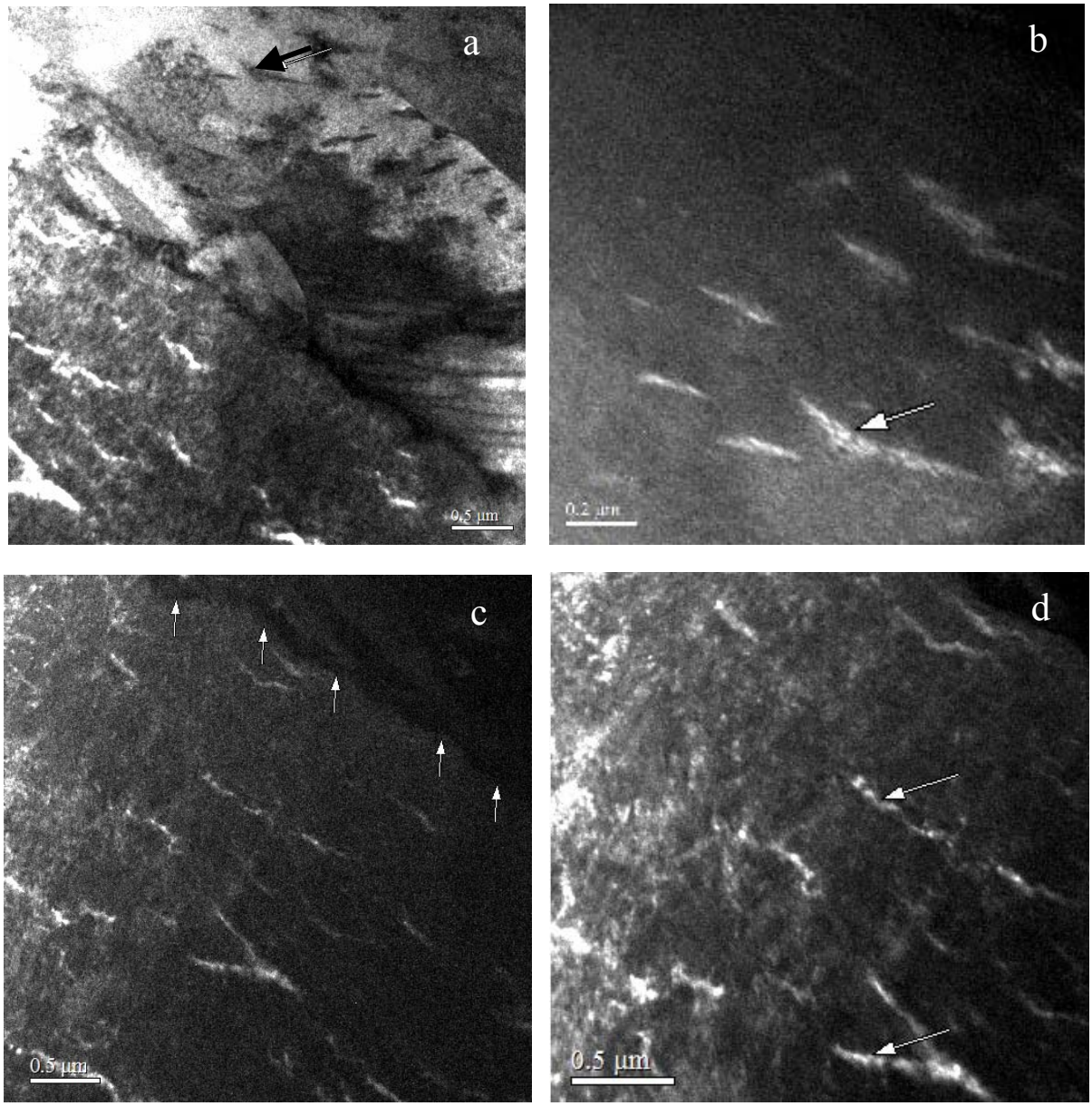

FIG. 7—*Metal-oxide interface of the Low-tin Zircaloy-4, irradiated for four cycles, in the same region as Fig. 5*a*; analysis for platelets precipitates.* a*) Bright field contrast of the interface indicating platelet type precipitates (black arrow).* b*) Dark field contrast of the region shown with the arrow at higher magnification. White arrow indicates the same platelet as in* a*. The dark field is obtained using the diffraction spot of platelets.* c*) The oxide side of the interface with the less dense regions, with equi-axed grains. Arrows indicate the limits of the interface.* d*) The same region as* c *at a different tilt and at higher magnification. Arrows indicate the less dense regions.*

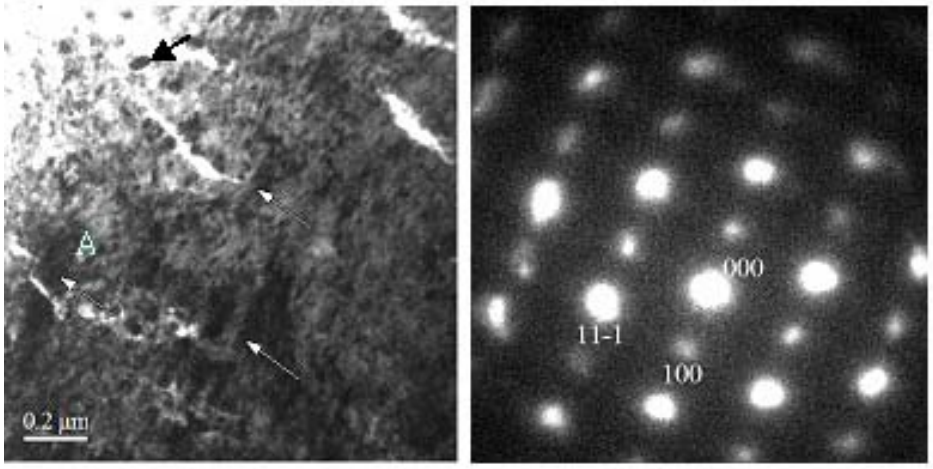

FIG. 8—*Bright field contrast of the oxide 3 μm away from the metal-oxide interface of the low-tin Zircaloy-4, irradiated for four cycles. White arrows indicate the columnar oxide grains. Black arrow indicates equi-axed grain. The diffraction pattern of the grain indicated by A is shown on the right image. This grain has a monoclinic structure. The zone axis for this orientation is [011].*

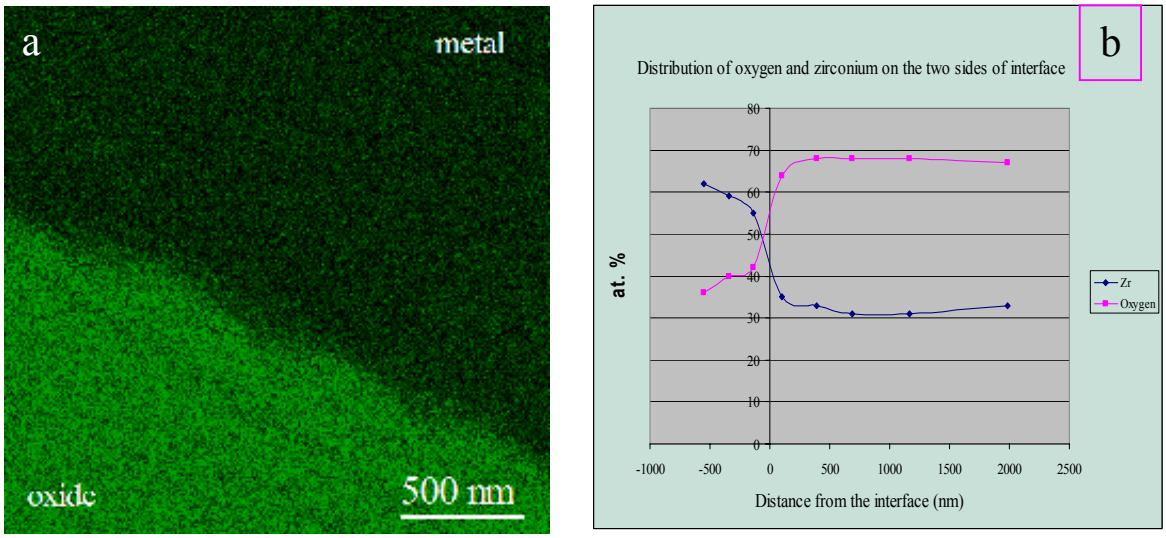

FIG. 9—a*) EDS map for oxygen in the same region as Fig. 5*a *and Fig. 7*a. b*) EDS point analysis for the distribution of oxygen and zirconium for the metal-oxide interface. Negative distance indicates the metal side of the interface.*

Zr-2.5% Nb Alloy

This alloy is commonly used for pressure tubes and as cladding material in the Russian reactors. It has been tested as a cladding material in the framework of a research project in collaboration with our laboratory. The material has shown satisfactory corrosion behavior; after three cycles in the reactor, the maximum oxide thickness of this alloy was 16 μm. The thin foil for the TEM observation of this material was also prepared by the FIB method. The overall view of the sample showing the geometry of the interface can be observed in Fig. 10*a*. The bright line

running from the top to the bottom of this image is an artefact of sample preparation due to the presence of cracks. The focused ion beam will drill a hole in the sample, at the end of the crack tip. This will cause a thinner cross-section in the region starting with the crack in the top of the TEM sample. The interface shows a morphology that is not observed in the two previous materials, especially in the case of low-tin Zircaloy-4 (Fig. 10*b*). The interface geometry is irregular in the Zr-2.5%Nb material, and it does not show a sinusoidal profile. It can be characterized as a "jigsaw" type interface. Cracks can be observed in the oxide region. The EDS maps of oxygen and Nb are shown in Fig. 11. Nb rich regions can be observed in the oxide. It has been shown by previous investigators that these Nb rich phases remain metallic in the oxide [16]. Our examinations of the oxide showed such a metallic diffraction pattern at a distance of 1 μm away from the interface. The structure of this phase with a cubic unit cell parameter of 0.37 nm could correspond to β-Zr slightly modified by oxygen dissolution; the stresses in the oxide could also induce such differences in d-spacing. The analysis of the interface at higher magnification shows that the limits of the interface are not very well defined, as compared with the case of low-tin material (Figs. 12 and 13).

The EDS point analysis of this material on the two sides of the interface shows a concentration of oxygen in the metal side of the interface that is much lower than those obtained for the low-tin Zircaloy-4 material. Since the point analysis of the standard Zircaloy-4 material is not possible, the comparison with that alloy is not available.

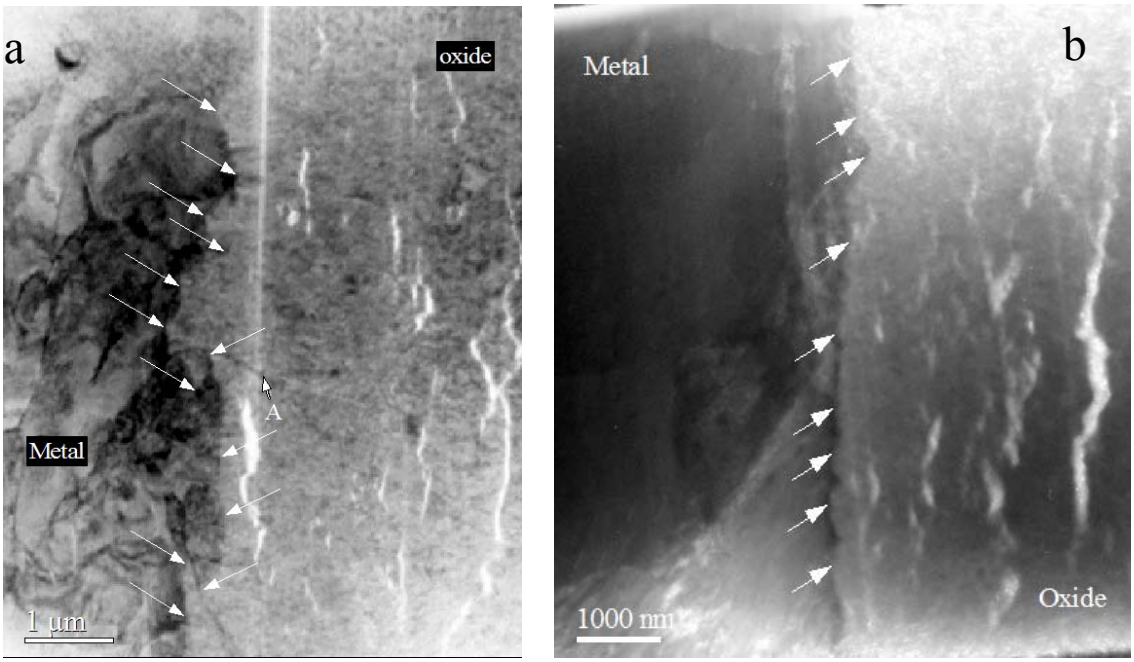

FIG. 10—a*) Metal-oxide interface of the Zr-2.5%Nb alloy after three cycles of irradiation. Arrows indicate the limits of the interface. The interface of this alloy has a very different profile compared to the low-tin Zircaoly-4. The metal-oxide interface shows regions that are rich in Nb (one such region is indicated by the letter A). Cracks can be observed in this alloy, in the oxide region.* b*) Metal-oxide interface of the low-tin Zircaloy-4 in the similar magnification for comparison.*

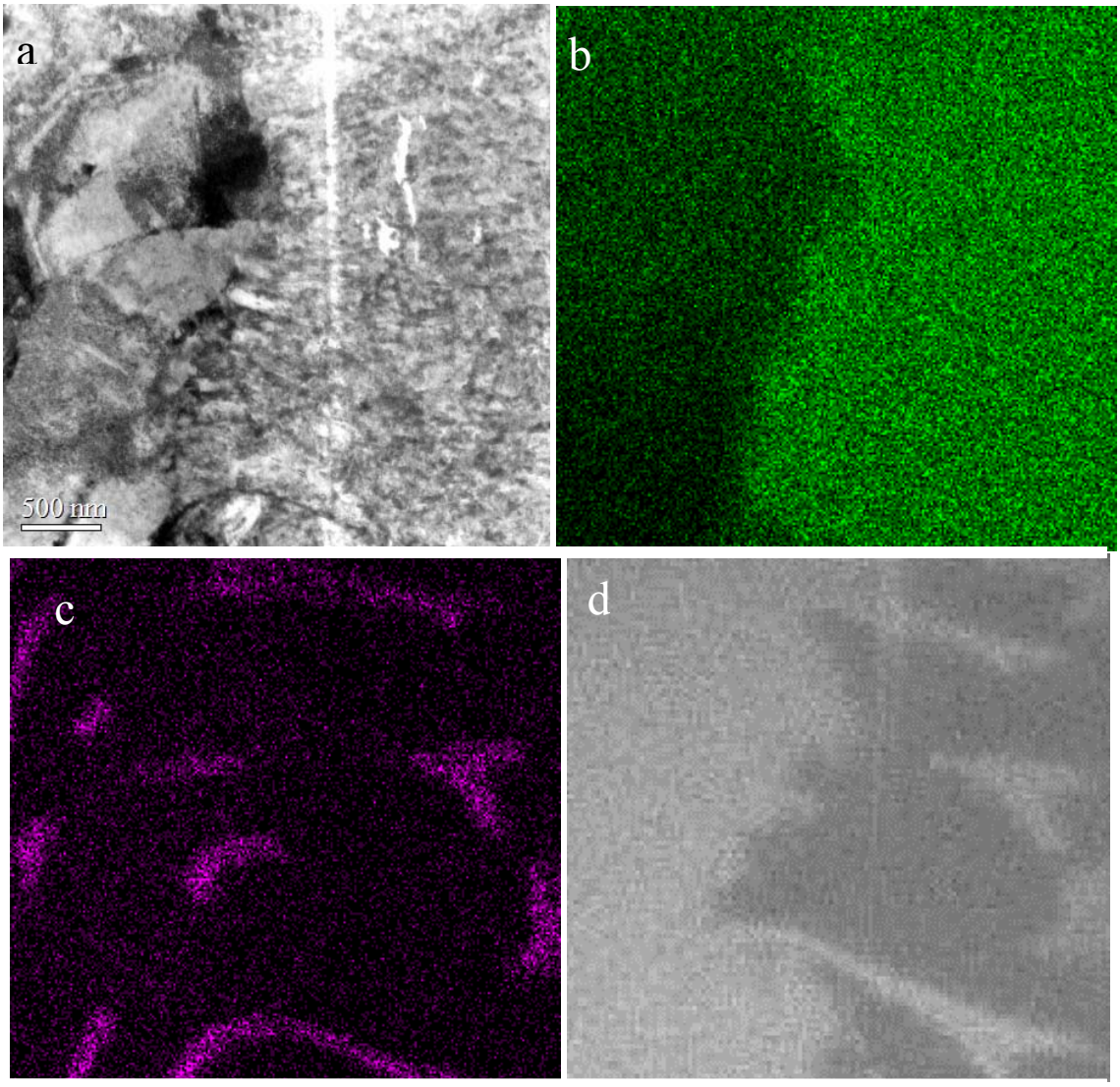

FIG. 11—*EDS map of metal-oxide interface of the Zr-2.5%Nb.* a*) Bright field contrast of the region mapped.* b*) Oxygen map.* c*) Nb map.* d*) The SEM image of the same region, taken at the final step of FIB sample preparation, before the removal of the sample from the bulk material.*

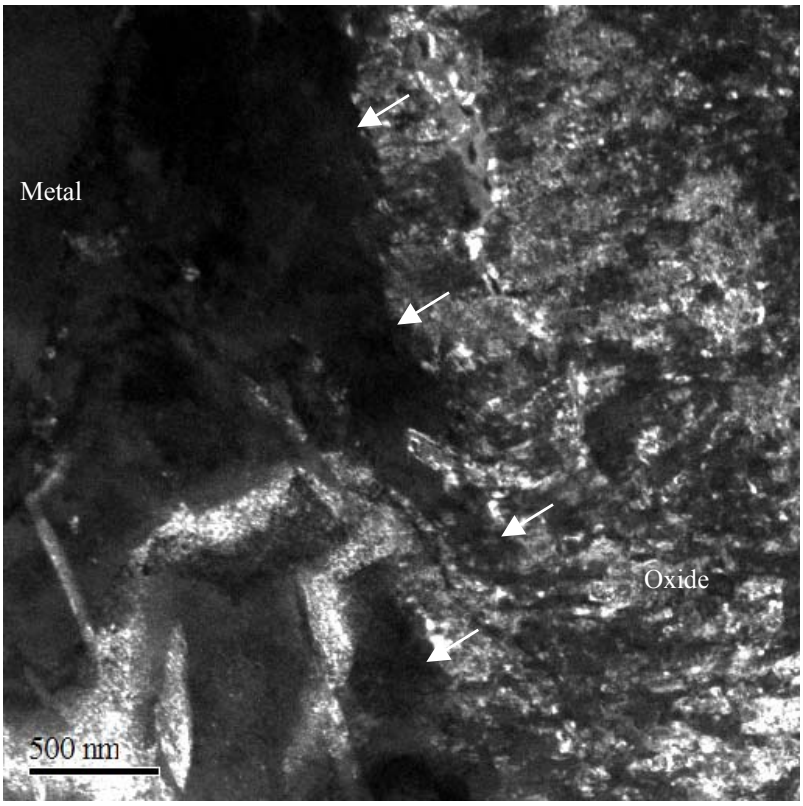

FIG. 12—*Dark field contrast of metal-oxide interface of the Zr-2.5%Nb alloy after three cycles of irradiation. Arrows point to the interface.*

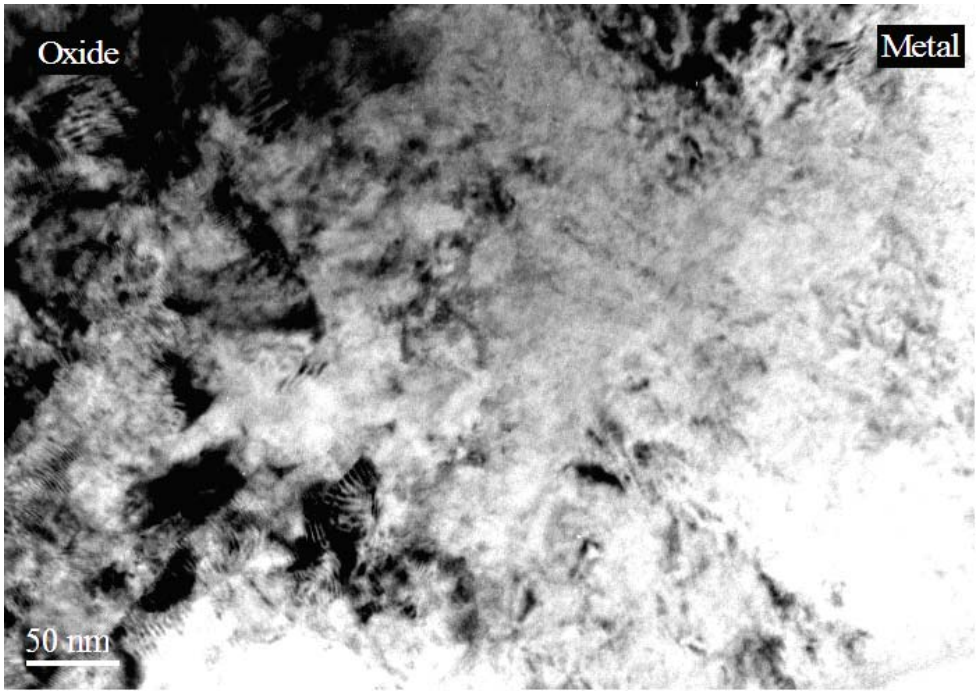

FIG. 13—*Bright field contrast of metal-oxide interface of the Zr-2.5%Nb, at higher magnification.*

Discussion

The possibility of analyzing the metal-oxide interface, particularly from FIB samples, is useful for studying the oxidation progress. Knowing that the oxide front will advance in the metal in the next step of oxidation, the analysis of the metal side of the interface can bring extra information about the process, the nature of the metal side of the interface influencing the nature of the oxide. The similarities of the two sides of the interface will bring hints about the mechanisms involved. As the samples in this experiment were available from a previous project and were not at the same rod elevation, it could be suggested that the direct comparison is not possible for the oxidation conditions due to the differences in temperature and fluence at the various elevations. However, the overall evaluation of these three materials can be performed based on different aspects of the oxidation process as follows:

Oxide Crystal Structure and Grain Morphology

Average ratios of different oxide phases at the interface can be obtained by X-ray diffraction, and the recent Synchrotron radiation facilities provide a resolution of the order of 0.2–1 μm [10]. The examination of phases present in the material by TEM should therefore focus on the correlation of the crystal structure with the microstructure.

In the present study, an attempt has been made to compare three different alloys and to observe the nature of the interface in all three cases. The observation of the three interfaces has shown that the prevailing oxide in all three materials is the monoclinic oxide. Tetragonal phase has been observed in the standard Zircaloy-4 in the grain boundaries of the monoclinic crystals. However, in the case of low-tin Zircaloy-4, no tetragonal phase has been detected. As the ratio of this phase to the monoclinic is usually low, it is not possible to conclude on the absence of the tetragonal phase in the low-tin Zircaloy-4. The long columnar grains of the oxide in this alloy have a monoclinic structure and are often surrounded by equi-axed grains. Because the cracks are observed at the grain boundaries of equi-axed grains, crack propagation must be easier through these boundaries, unlike columnar grains. Columnar monoclinic oxide grains seem to reduce the rate of propagation of cracks. They could be considered as whiskers in the oxide matrix. The presence of tetragonal phases has been correlated by some authors to a better resistance to oxidation [11], and the opposite is shown by other observations [10]. It would be expected that if the tetragonal phase would improve the resistance to oxidation, it would be due to its better mechanical properties. In the case of materials observed in this study there is no evidence that the small tetragonal phase present would enhance the oxidation resistance. This would imply that if in some cases the increase of the ratio of tetragonal phase is observed in the same time as the better resistance to oxidation, that case should be further examined, in order to find the correlation of the two observations and the possible influence of the tetragonal phase.

In general in phase transformation phenomena, columnar grains imply a continuous growth after a primary nucleation, without the presence of new nucleation sites in the material. If we assume that this fact is also valid for the oxidation phenomena, which are not the same type of phase transformation as solidification, for example, it would mean that the growth of the oxides in columnar regions is not interrupted and continues with a constant supply of oxygen. The grain boundaries of the oxide, in particular if they contain some equi-axed oxide grains, could provide such supply, due to the presence of faster roots for the diffusion of oxidizing species, such as cracks and pores. This situation could explain the oxidation condition of the Zircaloy-4 material.

The columnar structure, however, is not always present in this material, and at some regions the microstructure is equi-axed (Fig. 4).

The oxide structure of the Zr-2.5%Nb phase is different from the two other materials, as in the vicinity of the interface it consists of a composite structure containing metallic and oxide phases. The crystal structure of the oxide is again mainly monoclinic. The residual tetragonal phase at the interface of Zr-2.5%Nb has been observed by other investigations [10,17]. It has been shown that a small quantity of tetragonal phase is present in these oxides at the beginning of oxidation or in the vicinity of the interface. From the observations of the interface structure, it can be concluded that the oxidation resistance of this material is not directly due to the oxide crystal structure, and it may be to a certain extent due to the composite nature of the oxide of this material, the chemistry of the material also having its influence.

Oxidation of Hydrides

The low-tin Zircaloy-4 shows a large amount of hydride platelets in the metal side of the interface. Both radial and tangential hydrides are observed in this material. The shape and size of hydrides and their granular morphology in the metal side of the interface imply that the small cracks in the oxide could originate from these platelets. The presence of hydrogen in the cracks has not yet been checked, and work is in progress to perform this experiment. It is to be noted that the hydrogen hot extraction method shows the presence of hydrogen in the oxide [18,19]. And a recent study by SIMS has shown the presence of hydrogen in the oxide phase [20]. However, an accurate analytical examination of different regions of the oxide, including the less dense oxide is necessary to correlate the existence of hydrogen to the location of hydrides needles. It could be expected that when the oxidation front reaches the hydrides, the latter will also oxidize, leading to the formation of zirconia. The hydrogen can be expected to be released in any form, including water molecules. This would imply that the hydrogen detected by the above mentioned techniques in the oxide can be in different forms. The observation that the δ-hydride ($ZrH_{1.66}$) or a γ-hydride (ZrH) is absent in the metal side of the interface and a cubic zirconia or a ε-hydride ($ZrH_{1.95}$) is detected could have two explanations. Either the hydride in the vicinity of the interface is richer in hydrogen, or the hydride in this region oxidizes, leading to the equi-axed grains observed. The granular shape of hydrides has also been observed by other investigators [21], and it could be due to the lowest surface energy configuration of this phase in this form.

The other two materials did not show a large hydride distribution near the metal-oxide interface; therefore detailed examinations were not performed. The elevation of the segment for the standard Zircaloy-4 and the low hydrogen pick-up fraction of the Zr-2.5%Nb could be responsible for this situation (Table 1).

Stress Distribution and Crack Development

The mechanical properties of the oxide should be taken into consideration when the process of crack formation and propagation is examined. Although cracks can have several origins, this parameter should be considered in the analysis of the occurrence of the cracks, as one of the main factors responsible for crack formation.

The stresses developed in the oxides depend on the mechanism of oxidation, as an example, in the case of oxidation governed by the cation diffusion to the free oxide surface (e.g., some ferritic materials) it is claimed that the planar oxide layers will be stress free, and the stress build-up will be due to the subsequent formation of oxide grains within the defects and grain

boundaries of the former oxide scale [22]. In the case of zirconium alloys, as the oxidation takes place at the metal-oxide interface, the situation is different from the above case, and the volume difference of the metal and the oxide (Pilling-Bedworth parameter) do have an influence on the stress build-up in the layer.

If the external stresses are not taken into account, two types of stresses can exist in the oxide layer on a tube at constant temperature:

I. Stresses due to the volume differences between the metal and the oxide
II. A tensile stress, which can exist in the tube due to the diameter change as the oxide band is pushed away from the interface.

Volume Stresses—Linear interface in the case of the oxidation of zirconium will lead to very large compressive stresses, and it is known that the undulation observed in the interface of most alloys reduces the compressive stresses. Parise et al. [23] have modelled the interface by applying an undulated geometry and have calculated the levels of such stresses as a function of the amplitude of the undulations, in all directions in the tube. Compressive stresses as high as 2–4 GPa have been found for the oxide starting from the interface and reaching an asymptotic value of 2.5 GPa after a distance of 200–500 nm away from the surface.

From an in-situ examination of two zirconium alloys, it has been shown in a study by Petigny et al. [7] that the stresses at the interface can vary from one material to another. Values as high as –1800 MPa for Zr-1NbO and –200 to –500 MPa for Zircaoly-4 have been obtained at 743 K in that study. These stresses have dropped after a certain oxidation stage to lower values. A partially stabilized zirconia can show compressive strengths up to 2500 MPa. The failure of the oxide after a certain thickness could be due to the fact that the mechanical resistance of the oxide is reached at that level. The higher compressive values at the interface could be responsible for the fine cracks observed even at distances very close to the interface.

Tensile Stress Which Can Exist in the Tube Due to the Diameter—As explained above, the tube geometry in the case of the zirconium oxide will induce tensile stresses in the oxide band once it is pushed away by the new oxide. As an example for a cladding tube of 9.6 mm outer diameter, a band of oxide formed at this diameter and pushed to a 2 μm distance away from the interface will need to expand and develop a tensile stress of 75–150 MPa for the lower and higher values of elastic modulus of the oxide. The tensile strength of the zirconia ceramics of different structure varies between 85 and 350 MPa; therefore the thickness of the maximum oxide layer pushed away before failure can be determined according to the properties of the oxide formed. Therefore, even if the oxide at the interface would not show any compressive stresses (as could be the case in some regions of the Zr-2.5%Nb material), the material would fail in the case of the tube, due to these tensile stresses. The average thickness of the oxide layer observed for different materials in the tubes (e.g., [10]) will depend on the mechanical properties of the oxide and the nature of interface, the sum of the two stresses being responsible for the final failure stress in case both stress types act simultaneously.

In the absence of other failure sources (chemical dissolution, oxidized hydrides, radiation damages, etc.), the first cracks will occur at the positions where the local stress has reached the ultimate compressive or tensile resistance of the material, after which stage stress relaxation will occur.

The average stresses in the Zr-2.5%Nb are not available from in-situ studies, however from the examinations in this study it can be seen that the shape of the interface in the case of this

material is not undulated, but is similar to a jigsaw form; this allows the stress distribution to be optimized, since the increase of volume due to the oxide formation will be distributed over a larger volume of metal. The stress build up will therefore be much less than in the other morphologies. Also, the presence of a second phase in the oxide, which has a different mechanical property, will act as a composite component, which will raise the mechanical resistance of the oxide at the interface. Once the stresses are relaxed due to crack formation, in the case of this material the presence of Nb rich phase in the oxide, which could contain some metallic phase, the crack propagation will stop (Fig. 14). In this situation it is also expected that the interface will remain protected from the ingress of different oxidizing species.

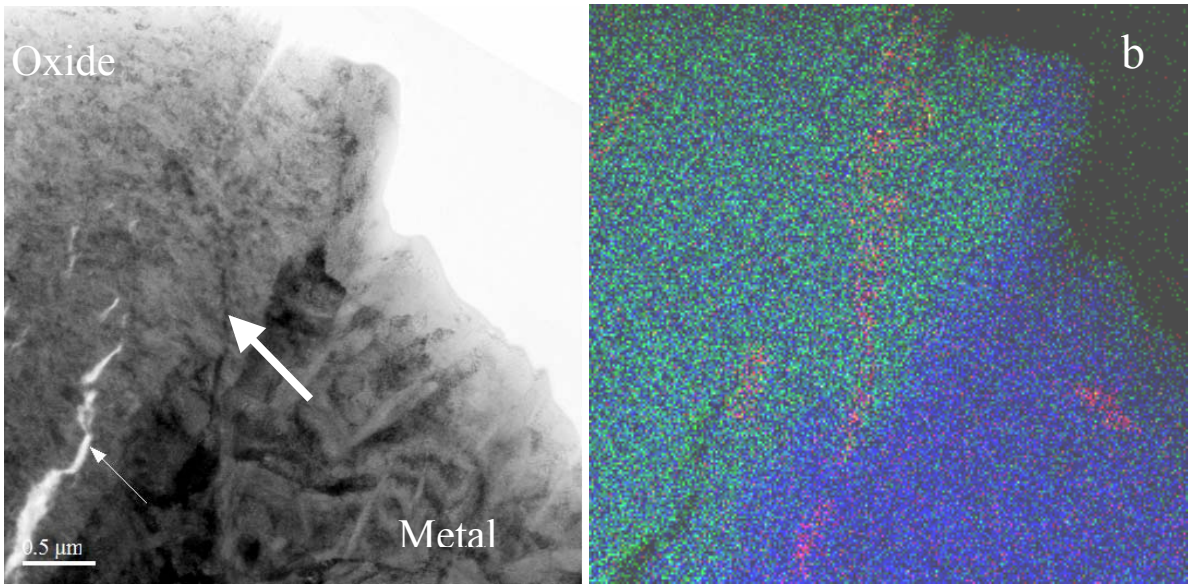

FIG. 14—a*) Bright field image of the metal-oxide interface of the Zr-2.5%Nb.* b*) EDS map of the same region. Blue: Zr, Green: oxygen, and purple: Nb. In this region a crack can be observed in the oxide region (shown by the small arrow in* a*). The Nb rich phase can be seen in the oxide region, also at the tip of the crack. Large arrow indicates the trace of the Nb rich region in the bright field image.*

In the case of low-tin Zircaloy-4, the situation seems different. The interface being sinusoidal, the stresses must be distributed homogeneously in the oxide side of the interface. The presence of SPP in the oxide should raise the mechanical resistance of the oxide, but the presence of equi-axed oxides seemingly due to the transformation of hydrides into oxide, will make the oxide susceptible to crack propagation, the equi-axed grains allowing the propagation of intergranular cracks more easily (Figs. 7 and 8). In this respect, the columnar monoclinic oxides show a better resistance to crack propagation. The homogeneous stress distribution at the interface and the presence of equi-axed regions for crack propagation could make the oxide in the case of this material less protective to ingress of oxidizing species. It could be expected that the large hydride distribution in the metal side of the interface would also reduce the plasticity of this side of the interface.

In the consideration of possible sites leading to crack formation and propagation, the original grain boundaries of the metal side of the interface can also be taken in to consideration; once

they oxidize, these regions could be a source of crack formation in the oxide, as the grain boundary of the metal subsists in the oxide.

Based on the data obtained about the geometry and the microstructure of the interface, a finite element calculation can be performed using the parameters above for obtaining the possible distribution of stresses in the material. The results can be validated by the comparison with the observations and by some local stress measurements on the thin foils.

Chemical Composition of the Interface

The mapping of the interface in this study is useful as it confirms the limits of the oxidized region, as observed from bright field and dark field contrasts. It cannot provide quantitative information about the distribution of different atoms. The point analysis of the interface as is presented in this study, however, can be taken as semi-quantitative data. The oxygen X-ray signal being easily absorbed by the Zr atoms (Z: 40), the thickness of the analyzed region in the TEM will be very critical for the measurements, and although in the TEM the thin foil approximation will simplify the correction calculations, in the case of zirconium, the oxygen concentration could be false due to the thickness of the foil. A pure zirconia standard has been used to check this problem. Also, from sputtered thin films the relation of the thickness and composition has been calibrated. Using these measurements, the value for the thickness should be below 60 nm. The data obtained from thin foils can therefore at least be considered as semi-quantitative. In this respect, FIB samples are more reliable as the thickness variations of the foil are much less than in the case of the samples prepared by conventional ion milling.

The concentration gradient obtained in the case of the low-tin Zircaloy-4, will reveal the high concentration of the oxygen in the metal side of the interface. Even if the material is thicker than the value above, the oxygen absorption by zirconium would lead to a real concentration that would be higher than that measured. The thickness of the thin foil has been appropriate for this measurement. A high concentration of oxygen in the metal side of the interface would imply a faster rate of oxidation [25,26], as the dissolved oxygen is shown to raise the oxidation rate.

In the case of Zr-2.5%Nb alloy we obtained a rapid drop of oxygen gradient in the metal side of the interface (not shown here). Although this is in agreement with the behavior of this material and the very low diffusion rate of oxygen as compared with the other two materials, it should be further examined to rule out the above mentioned thickness effect.

The oxygen solubility of the α-Zr is 28.6 At% up to 500°C, the observation of a gradient showing higher concentration of oxygen, would conclude that the interface in the case of such phenomena is not a monolayer. The oxygen gradient at this distance from the interface has not been examined by other studies. It could be expected that the region near the interface represents a non-stoichiometric oxide.

Effect of Irradiation

The effect of irradiation on the oxide could be subdivided into three main aspects:

I. The effect of radiation damage present in the metal substrate on the oxide formed after long term reactor stay
II. The effect of irradiation on the microstructure of the existing oxide after long term stay in the reactor

III. the effect of irradiation on the chemical species present in the reactor and their interaction with the oxide, leading to microstructural changes in the oxide and to a change of oxidation potential in the metal

The above aspects will be discussed separately:

I. The Radiation Damage of the Substrate—The irradiation damage present in the metal, the point defects present in the substrate, as well as the modification of precipitate structure and composition have been examined extensively (e.g., [27]). The dissolution of the SPP has been observed in many alloys, and it is clear that in the case of irradiated metal, this will be a parameter which will differ from an unirradiated substrate. The composition of the matrix will also be totally different. These two factors are, without ambiguity, causes of change of oxidation rate. An example which has shown the effect of these two factors can be seen in the study by Isobe et al. [28]. Another parameter that should be taken into consideration is the change of microstructure of the α-Zr matrix due to irradiation. When the dislocation density increases to an extent that the subgrains are formed and the material becomes brittle, this change in microstructure can modify the behavior of the substrate and could cause a change in oxidation behavior.

In the case of low-tin Zircaloy-4, it has been observed that stacking fault tetrahedra are formed in the vicinity of the interface. These features could have an influence on the oxidation rate change. Further oxidation studies on other irradiated material are necessary to demonstrate the possibility of such correlations.

II. The Effect of Irradiation on the Microstructure of the Existing Oxide and Subsequent Change of Oxidation Rate—In previous studies on Zircaloy-4 [29–31] and on Zr-2.5%Nb CANDU® pressure tubes [32], growth of oxide grains had been observed at the water side position. In this study, only a very small grain growth could be observed from the metal-oxide interface to the water side oxide. Although the example of the Zircaloy-4 presented here was selected from a position with lower fluence, the same examinations performed on Zircaloy-4 with a β-quench heat treatment having an oxide thickness of 55 μm showed columnar oxide in the water side oxide, and the width of columnar grains were about 25 nm as it was seen in the materials presented here. The focus in this study being on the metal-oxide interface of the materials examined, there are not sufficient statistics available to comment further on this difference of observations. Certain beam sensitivity is mentioned in the case of Zircaloy-4 studies [29–31] that were not observed in the present examinations. Furthermore, the TEM samples in the case of these materials were selected in the direction parallel to the interface. These samples were therefore perpendicular to the columnar grains present in the material and growing in the direction of growth of oxide. It is thus difficult to compare these two sets of data with each other. The difference existing between the Zr-2.5%Nb alloy examined in this study and that of Ref. [32] can be in their heat treatment and in the differences in the microstructure of the two materials or in the oxidation conditions.

III. The Effect of Irradiation on the Chemical Species Present in the Oxide and Their Interaction with the Oxide—Previous investigations have shown the effect of change of oxide chemistry as a consequence of the interaction with the water chemistry and due to the redistribution of the alloying elements in the oxide. This factor is of great importance on the structure of the oxide and its permeability to oxidizing species. The EDS point analysis is not

adapted to the study of traces of elements present in the coolant water. Also, a direct cause-effect study is not possible without the information about the water chemistry. The effect of redistribution of the alloying elements in the oxide has been reported by Iltis et al. [30], and it has been shown that the oxide microstructure is different in the areas surrounding the precipitates. Few precipitates were observed in the oxide films examined in our studies. Further experiments in this respect are planned for a future study.

Conclusions

Metal-oxide interfaces of a standard Zircaloy-4 and a low-tin Zircaloy-4 irradiated for four cycles and a Zr-2.5%Nb irradiated for three cycles in a PWR were examined by TEM. The geometry of the interface, crystal structure of the oxide grains and their morphology, and the composition of each material at the two sides of the interface were examined. The Zr-2.5%Nb shows features that can be considered substantially different from the other two materials.

The interface of Zr-2.5%Nb shows an irregular profile that can be described as "jigsaw" form compared to the other two materials. The oxide layer in this material shows metallic grains at a distance of 1 μm from the interface. These grains can be characterized as Nb-rich cubic phase, most probably a β-zirconium.

The EDS point analysis of the interface of this material has shown that it contains less dissolved oxygen in the metallic side, compared to the low-tin Zircaloy-4. This finding and the geometry of the interface in this material could suggest that the high corrosion resistance of this alloy is due to a better stress distribution at the interface, leading to a lower crack density at the vicinity of the interface, and to slower oxygen diffusion through the metal. The relation of these two features to each other should be studied further.

In the case of low-tin Zircaloy-4, the hydride platelets present in the metal side showing a higher density than the other two materials led to small equi-axed oxide grains. These grains can make the material more susceptible to crack propagation. Also, the undulated geometry of the interface of this material plays a role on the relaxation of stresses, but not to the same extent as it is possible in the case Zr-2.5%Nb. This will further increase the possibility of the oxide failure by cracking. The interface of this material shows higher oxygen content in the metal side.

The Zircaloy-4 material shows a columnar structure, however at certain regions of the interface other types of grains are observed. This material showed a fine tetragonal phase at the interface, in the grain boundaries of the columnar oxides. Intergranular oxidation was observed in this material.

Acknowledgments

The authors wish to thank Dr. Armin Hermann for providing the irradiated materials and Mr. Roland Bruetch for the SEM measurements of the oxide thickness. This work has been supported by UAK Switzerland.

References

[1] "Waterside Corrosion of Zirconium Alloys in Nuclear Power Plants," IAEA-TECDOC-996, January 1998, IAEA.

[2] Urbanic, V. F., Choubey, R., and Chow, C. K., "Investigation of Variables that Influence Corrosion of Zirconium Alloys during Irradiation," *Zirconium in the Nuclear Industry: 9th*

International Symposium, *ASTM STP 1132*, C. M. Eucken and A. M. Garde, Eds., ASTM International, West Conshohocken, PA, 1991, pp. 665–682.

[3] Garzarolli, F., Broy, Y., and Busch, R. A., "Comparison of the Long-Term Corrosion Behaviour of Certain Zr Alloys in PWR, BWR and Laboratory Tests," *Zirconium in the Nuclear Industry: 11th International Symposium, ASTM STP 1295*, E. R. Bradley and G. P. Sabol, Eds., ASTM International, West Conshohocken, PA, 1996, pp. 850–864.

[4] Franklin, D., and Li, C-Y., "Effects of Heat Flux and Irradiation-Induced Changes in Water Chemistry on Zircaloy Nodular Oxidation," *Zirconium in the Nuclear Industry: 7th International Symposium, ASTM STP 939*, R. B. Adamson and L. F. P. Van Swam, Eds., ASTM International, West Conshohocken, PA, 1987, pp. 206–223.

[5] Grandjean, A. and Serruys, Y., "Metal and Oxygen Mobilities During Zircaloy-4 Oxidation at High Temperature," *Journal of Nuclear Materials*, Vol. 273, No. 1, 1999, pp. 111–115.

[6] Jacquot, T., Guillen, R., François, M., Bourniquel, B., and Senevat, J., "Residual Stress of Monoclinic Zircon Obtained by X-Ray Diffraction in ZY4 Oxidized Cladding Tubes," *Materials-Science-Forum*, Vol. 228, 1996, pp. 845–50.

[7] Pétigny, N., Barberis, P., Lemaignan, C., Valot, C. H., and Lallemant, M., "In Situ XRD Analysis of the Oxide Layers Formed by Oxidation at 743 K on Zircaloy 4 and Zr-1NbO," *Journal of Nuclear Materials*, Vol. 280, 2000, pp318–330.

[8] Pêcheur, D., "Oxidation of β-Nb and Zr/Fe, V_2 Precipitates in Oxide Films Formed on Advanced Zr-Based Alloys," *Journal of Nuclear Materials*, Vol. 278, 2000, pp. 195–201.

[9] Godlewski, J., Gros, J. P., Lambertin, M., Wadier, J. F., and Weidinger, H., "Raman Spectroscopy Study of the Tetragonal-to-Monoclinic Transition on Zirconium Oxide Scales and Determination of Overall Oxygen Diffusion by Nuclear Microanalysis of O^{18}," *Zirconium in the Nuclear Industry: 9th International Symposium, ASTM STP 1132*, C. M. Eucken and A. M. Garde, Eds., ASTM International, West Conshohocken, PA, 1991, pp.416–436.

[10] Yilmazbayhan, A., Motta, A. T., Comstock, R. J., Sabol, G. P., Lai, B., and Cai, Z., "Structure of Zirconium Alloy Oxides Formed in Pure Water Studied with Synchrotron Radiation and Optical Microscopy: Relation to Corrosion Rate," *Journal of Nuclear Materials*, Vol. 324, 2004, pp. 6–22.

[11] Anada, H., Takeda, K., Hagi, S., Murata, T., Oe, A., and Miyashita, T., "Out-of-Pile Corrosion Behaviour and Corrosion Mechanism of NDA for High Burn-up Fuel of PWR," *Proceedings of the ANS International Topical Meeting on LWR Fuel Performance, IAEA*, 10–13 April 2000, Park City.

[12] Cox, B., "A Mechanism for the Hydrogen Uptake Process in Zirconium Alloys," *Journal of Nuclear Materials*, Vol. 264, 1999, pp 283–294.

[13] Wikmark, G., Rudling, P., Lehtinen, B., Hutchinson, B., Oscarsson, A., and Ahlberg, E., "The Importance of Oxide Morphology for the Oxidation Rate of Zirconium Alloys," *Zirconium in the Nuclear Industry: 11th International Symposium, ASTM STP 1295*, E. R. Bradley and G. P. Sabol, Eds., ASTM International, West Conshohocken, PA, 1996, pp. 55–73.

[14] Cox, B., Wong, Y. M., "A Hydrogen Uptake Micro-Mechanism for Zr Alloys," *Journal of Nuclear Materials*, Vol. 270, 1999, pp 134–146.

[15] Abolhassani, S., Schäublin R., Groeschel F., and Bart, G., "AEM and HRTEM Analysis of the Metal-Oxide Interface of Ziraloy-4 Prepared by FIB," *Proceeding of Microscopy and Microanalysis 2001*, Long Beach, CA, August 5–9, 2001, pp. 250.

[16] Lin, Y. P., and Woo, O. T., "Oxidation of β-Zr and Related Phases in Zr-Nb Alloys: An Electron Microscopy Investigation," *Journal of Nuclear Materials*, Vol. 277, 2000, pp. 11–27.
[17] Khatamian, D., and Lalonde, S. D., "Crystal Structure of Thin Oxide Films Grown on Zr-Nb Alloys Studied by RHEED," *Journal of Nuclear Materials*, Vol. 245, 1997, pp. 10–16.
[18] Hermann, A., "Thermal Behaviour of Hydrogen in Zircaloy Corrosion Layers," *Journal of Nuclear Materials*, Vol. 302, 2002, pp. 217–219.
[19] Hermann, A., Wiese, H., Bühner, R., Steinemann, M., and Bart, G., "Hydrogen Distribution Between Fuel Cladding Metal and Overlying Corrosion Layers," *Proceedings of the ANS International Topical Meeting on LWR Fuel Performance, IAEA*, 10–13 April 2000, Park City, pp. 372–384.
[20] Oskarsson, M., Ahlberg, E., Södervall, U., Andersson, U., and Pettersson, K., "Pre-Transition Oxidation Behaviour of Pre-Hydrated Zircaloy-2," *Journal of Nuclear Materials*, Vol. 289, 2001, pp. 315–328.
[21] Chung, H. M., Daum, R. S., Hiller, J. M., and Billone, M. C., "Characteristics of Hydride Precipitation and Reorientation in Spent Fuel Cladding," *Zirconium in the Nuclear Industry: 13th International Symposium, ASTM STP1423*, G. D. Moan and P. Rudling, Eds., ASTM International, West Conshohocken, PA, 2002, pp. 561–582.
[22] Krishnamurthy, R. and Srolovitz, D. J., "Stress Distribution in Growing Oxide Films," *Acta Materialia*, Vol. 51, 2003, pp. 2171–2190.
[23] Parise, M., Sicardy, O., and Cailletaud, G., "Modelling of the Mechanical Behaviour of the Metal-Oxide System During Zr Alloy Oxidation," *Journal of Nuclear Materials*, Vol. 256, 1998, pp. 35–46.
[24] Ritchie, I. G. and Atrens, A., "The Diffusion of Oxygen in α-Zirconium," *Journal of Nuclear Materials*, Vol. 67, 1977, pp. 254–264.
[25] Pemsler, J. P., "Studies on the Oxygen Gradients in Oxidizing Materials. The Oxidation of Oxygen-Saturated Zirconium," *Journal of the Electrochemical Society*, Vol. 113, 1966, pp. 1241–1244.
[26] Harada, M., Kimpara, M., and Abe, K., "Effect of Alloying Elements on Uniform Corrosion Resistance of Zirconium-Based Alloys in 360°C Water and 400°C Steam," *Zirconium in the Nuclear Industry: 9th International Symposium, ASTM STP 1132*, C. M. Eucken and A. M. Garde, Eds., ASTM International, West Conshohocken, PA, 1991, pp.368–391.
[27] Abolhassani, S. Gavillet D., Groeschel F., Jourdain P., and Zwicky H. U., "Recent Observations on the Evolution of the Secondary Phase Particles in Zircaloy-2 under Irradiation in a BWR up to High Burn-Up," *Proc. of the International Topical Meeting on Light-Water-Reactor Fuel Performance, IAEA*, April 10–13, 2000, Park City, Utah, p. 470.
[28] Isobe, T., Murai, T. and Mae, Y., *Zirconium in the Nuclear Industry: 11th International Symposium, ASTM STP 1295*, ASTM International, West Conshohocken, PA, Garmisch-Partenkirchen, 1996, pp. 203–217.
[29] Iltis, X., Lefebvre, F., and Lemaignan, C., "Microstructural Study of Oxide Layers Formed on Zircaloy-4 in Autoclave and Reactor-Part I: Impact of Irradiation on the Microstructure of Zirconia Layer," *J. Nucl. Mater.*, Vol. 224, 1995, pp. 109–120.
[30] Iltis, X., Lefebvre, F., and Lemaignan, C., "Microstructural Study of Oxide Layers Formed on Zircaloy-4 in Autoclave and Reactor-Part II: Impact of the Chemical Evolution of Intermetallic Precipitates on their Zirconia Environment," *J. Nucl. Mater.*, Vol 224, 1995, pp. 121–130.

[31] Iltis, X., Lefebvre, F., and Lemaignan, C., "Microstructure Evolutions and Iron Redistribution in Zircaloy Oxide Layers: Comparative Effects of Neutron Irradiation Flux and Irradiation Damages," *Zirconium in the Nuclear Industry: 11th International Symposium, ASTM STP 1295*, E. R. Bardley and G. P. Sabol, Eds., ASTM International, West Conshohocken, PA, 1996, pp.242–264.

[32] Woo, O. T., Lin, Y. P., and Khatamian, D., "Oxide Mircostructure and Deuterium Ingress in Zr-2.5Nb CANDU® Pressure Tubes," *Materials at High Temperatures*, Vol. 20, 2003, pp. 593–600.

Appendix I

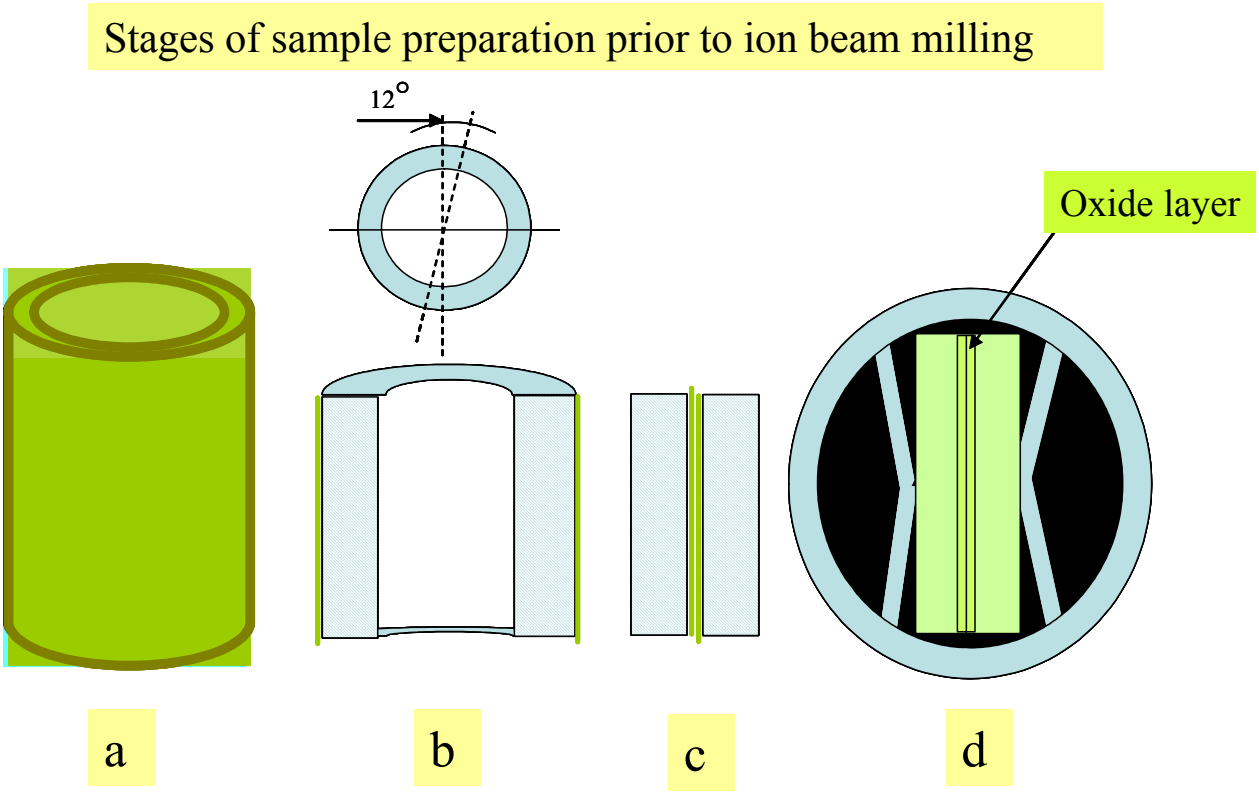

a. A disc segment of fuel rod with a height of 3–5 mm is cut and defueled in the hot-cell. The ring of cladding is subsequently cleaned to remove the residual fuel.

b. It is then cut in the hot-cell into small segments 2 mm wide, in the direction parallel to the tube axis. The segment is cleaned from the inner wall in order to remove the traces of fission products penetrated into the inner wall of the cladding. The segment is subsequently cleaned in ultrasonic bath in the hot-cell in order to remove the remaining loose contamination and is measured for the level of activity. The level of activity of the samples after the last decontamination is an important parameter, as a long sample preparation is still necessary after the last stage in the hot-cell.

c. The samples are cut again outside the hot cell to the appropriate dimensions and subsequently joined together with the oxide sides facing each other.

d. They are then mounted on a 3 mm TEM holder. The thickness of the foil is subsequently reduced to a sufficient size for ion milling (20–30 μm).

Appendix II

TABLE A.1—*Crystallographic parameters of the oxide structures, possible hydride structures, and possible metallic phases considered for the analysis of the interface.*

Material	Crystal System	a nm	b nm	c nm	β	Space Group	XPDF* No.
ZrO_2	Monoclinic	0.53129 (4)	0.52125 (4)	0.51471 (5)	99.218(8)	P21/a (14)	37-1484
	Cubic	0.509				Fm3m (225)	7-997
	Tetragonal	0.364		0.527		P42/nmc (137)	42-1164
γ-ZrH	Tetragonal	0.45957		0.49686		$P4_2/n$ (86)	34-0690
δ-$ZrH_{1.66}$	Cubic	0.4781				Fm3m (225)	34-0649
ε-$ZrH_{1.950}$	Tetragonal	0.49789 (9)		0.44508 (9)		F4/mmm	36-1339
ZrH_2	Tetragonal	0.352(3)		0.4449 (3)		I4 (79)	73-2076
α-Zr	hexagonal	0.3232		0.5147		P63/mmc (194)	5-665
β-Zr	bcc	0.35453				Im3m (229)	34-657
β-Nb	bcc	0.3336					

* XPDF: X-ray Powder Diffraction File.